RESTRICTED INVESTIGATION REPORT 1411R

CSIRO

INSTITUTE OF ENERGY AND EARTH RESOURCES

Division of Mineral Physics

HYSTERESIS PROPERTIES OF SIZED DISPERSED MONOCLINIC PYRRHOTITE GRAINS

D.A. CLARK

P.O. Box 136
North Ryde, NSW
AUSTRALIA 2113

APRIL, 1983

TABLE OF CONTENTS

LIST OF TABLES

LIST OF FIGURES

Fig. 5 AF demagnetisation curves of saturation remanence for selected sized pyrrhotite specimens.

Fig. 6 AF coercivity spectra for specimens NRC, R4, R8 and R12.

Fig. 7 AF coercivity spectra for specimens R14, R16, R17 and R18.

Fig. 8 Bilogarithmic plot of coercive force versus grain size for sized pyrrhotite specimens.

1. INTRODUCTION

In the past rock magnetic studies have concentrated on the properties of titanomagnetite and haematite, as these are the principal carriers of remanence in the rocks most studied by palaeomagnetists. By comparison very little is known about the rock magnetism of pyrrhotite. However pyrrhotite is dominantly responsible for anomalous magnetic signatures in many mineralised terrains and orebodies. Lack of knowledge of the magnetic properties of pyrrhotite inhibits reliable interpretation of magnetic anomalies in these areas.

In an attempt to correct this deficiency the hysteresis properties of sized dispersed monoclinic pyrrhotite grains have been determined. Monoclinic pyrrhotite is the only stable strongly magnetic phase in the pyrrhotite group. The properties measured were: low-field susceptibility and its variation with field strength, coercive force, coercivity of remanence, coercivity of remanence acquisition, median destructive field and saturation remanence.

The results show a strong grain-size dependence of magnetic properties, analogous to that of other magnetic materials. Overall pyrrhotite of grain-size smaller than 100 μm is magnetically hard (i.e. it has high coercivity). Hard magnetic materials are capable of bearing intense, stable remanence.

Theoretical analysis of the rock magnetism of pyrrhotite and the implications of the experimental data for magnetic petrophysics and palaeomagnetism of pyrrhotite-bearing rocks will be presented in another report.

2. SAMPLE PREPARATION

After perusal of thermomagnetic curves of numerous natural pyrrhotite-rich samples, the massive pyrrhotite ore from Mt. Bonnie was selected for preparation of magnetic separates from which distinct grain-size fractions were produced. This ore was chosen because the k-T and J_s-T curves indicated monoclinic 4C pyrrhotite as the only magnetic mineral present and because of the near-perfect reversibility of the thermomagnetic curves, even after heating in air to ~600°C (Fig. 1). Reversibility of the curves indicates negligible chemical change even under the extreme experimental conditions encountered during the k-T runs. It was therefore hoped that the pyrrhotite would similarly resist oxidation during crushing, sizing and dispersal in an inert matrix.

It should be noted that the bulk pyrrhotite appears to be unremarkable in its magnetic properties, although it is unusually stable and resistant to oxidation. It is well known that the reactivity of natural pyrrhotites is very sensitive to composition (stoichiometry and impurities). For instance hand samples or polished surfaces of some samples may remain fresh for years whereas other samples, which are crystallographically indistinguishable, may literally tarnish before the observer's eyes. The Mt. Bonnie pyrrhotite may therefore be stabilised by minor impurities, or the stability may stem from the well-annealed nature of the grains as indicated by the metamorphic texture of the ore.

Mt. Bonnie is a stratabound ore deposit occurring within the Lower-Proterozoic Golden Dyke Formation of the Pine Creek

Geosyncline, N.T. Measurement on oriented drill core samples supplied by Geopeko Ltd. indicate the presence of an intense, stable remanence which is highly oblique to the present field direction, clearly representing an ancient magnetisation. Magnetic modelling indicates that the remanence determined from the drill-core samples is representative of the body as a whole and accounts well for the observed magnetic anomaly (R. Duffin, pers. comm.).

I am indebted to Dr J. McAndrew for the petrographic description of the sample from which the pyrrhotite grain-size fractions were prepared (Appendix).

The ore was crushed and the magnetic fraction extracted. The magnetic extract was separated into grain-size fractions ranging from ~80μm to less than 3μm using a Bahco dust analyser. The samples were then stored in stoppered vials for several months. Standard procedures which are normally followed in order to minimise oxidation (for instance grinding under acetone) were specifically avoided. This is because they probably would not be effective when dealing with reactive pyrrhotite, and the inevitable exposure of the grains to oxidation during characterisation of the samples and specimen preparation would invalidate the analysis of the samples. Instability of properties of the artificial specimens could render results obtained useless. Reliance was therefore placed on the fortuitously unreactive nature of the Mt. Bonnie pyrrhotite, and this confidence was amply justified by the results.

Immediately before preparation of the synthetic specimens the pyrrhotite grain-size fractions were analysed by X-ray diffraction revealing essentially the presence of 4C pyrrhotite only in fractions ranging from the coarsest to the finest grains. No magnetite, maghaemite or haematite was detected, the only contaminant found being chalcopyrite up to a few percent in the finest fraction.

A small portion of each grain-size fraction was examined microscopically in order to determine the grain-size distributions. Typical photographs of these fractions are shown in Fig. 2. Care was taken to homogenise the mixture by adding the pyrrhotite and the resin a little at a time and by thorough stirring. Before adding the pyrrhotite to the resin the pyrrhotite powder was mixed with 0.3g of pure quartz sand grains to break up the larger clumps of pyrrhotite grains during dispersal. Subsequent stirring successfully smeared remaining aggregates of grains throughout the matrix, but some clumping on a microscopic scale inevitably persisted. The resin was sufficiently viscous to prevent significant settling of the pyrrhotite grains during hardening.

Because of the limited quantity of material available only very dilute pyrrhotite dispersions were prepared. Only in the case of the coarsest fraction (NRC) could more than one specimen be prepared to allow investigation of the effect of concentration on the magnetic properties.

After completion of the magnetic measurements the bases of 3 specimens (NRC2, R4 and R17) were polished and examined under high magnification in reflected light. The observations showed that the pyrrhotite grains, even the finest, remained

absolutely uncorroded and untarnished. The measured magnetic properties of the specimens are therefore considered to represent the properties of pure monoclinic 4C pyrrhotite with grain sizes corresponding to those cited in Table 1. Further evidence of some contamination of the pyrrhotite powders with grains of other minerals was provided by observation of specimen R17.

3. LOW-FIELD SUSCEPTIBILITY AND THE RAYLEIGH PARAMETER

The low field susceptibility in ~1 Oersted was measured using a low frequency (211 Hz) transformer bridge (Ridley and Brown, 1980), calibrated using $MnSO_4.H_2O$ as a standard. After a small correction for the diamagnetic susceptibility of the matrix, the results were normalised to unit mass of pyrrhotite to obtain the mass susceptibility of the pyrrhotite. A density of 4.6 g/cm^3 was assumed for calculation of the volume susceptibility. Because of contamination of the finer pyrrhotite fractions with non-magnetic grains the mass of pyrrhotite was actually determined from saturation magnetisation measurements (see Section 4).

The sizes of ~30 grains were measured and mean sizes and standard deviations calculated (Table 1). In Table 1 the mnemonics refer to ring numbers in the Bahco dust analyser, except for the No Ring Coarse (NRC) and No Ring Fine (NRF) fractions. Although there is some overlap of the grain-size distribution between neighbouring fractions, overall the separation was quite satisfactory.

The microscopic examination revealed the presence of minor non-pyrrhotite phases in the separates, indicating that magnetic separation did not completely remove all gangue and non-magnetic sulphides. Occasional large grains of contaminant in the finer fractions, however, may significantly affect normalisation of susceptibility and saturation magnetisation to unit mass or volume of pyrrhotite.

Small quantities (~0.1g) of each grain-size fraction were then accurately weighed and dispersed in epoxy resin to produce cylindrical specimens of 25mm diameter and 22mm height.

The field dependence of susceptibility was determined using an Arun Electronics susceptibility bridge designed by C. K. Radhakrishnamurty. This bridge operates at ~250Hz and allows variation of the peak applied field from 0 to ~20 oe The field was calibrated using a Hall effect gaussmeter and linearity of the instrument in the range 0-15 Oe was verified using the paramagnetic susceptibility calibration specimen which had susceptibility comparable to the strongest dispersed pyrrhotite specimen (NRC 2).

When the maximum applied field is considerably less than the bulk coercive force of a ferromagnetic or ferrimagnetic substance the Rayleigh relationships are obeyed (Chikazumi and Charap, 1978, p.296ff.). The initial magnetisation curve is quadratic in applied field H

$$J = \chi H + \eta H^2 \qquad (1)$$

where χ is the initial or reversible susceptibility and η is the Rayleigh parameter. If the field is increased to a maximum value H_1 ($<<H_c$) and then decreased, hysteresis occurs. The remanence acquired in H_1 is given by

$$J_r = \eta H_1^2/2 \qquad (2)$$

The hysteresis loop in the Rayleigh region (Rayleigh loop) has the form of two parabolic arcs with equations

$$J = (\chi+\eta H_1)H + \eta(H^2-H_1^2)/2 \quad \text{(ascending branch)} \qquad (3)$$

$$J = (\chi+\eta H_1)H - \eta(H^2-H_1^2)/2 \quad \text{(descending branch)} \qquad (4)$$

When the applied field is sinusoidal $H = H_1 \sin\omega t$, M lags behind H due to the hysteresis and the waveform is distorted with the introduction of odd harmonics. Substituting $H = H_1 \sin\omega t$ into (3) and (4) and performing a Fourier analysis on $B = H + 4\pi J$ gives

$$B = B_\omega \sin(\omega t-\delta) + B_{3\omega} \sin 3\omega t + \ldots \qquad (5)$$

where

$$\tan\delta = 16\eta H_1/3(1+4\pi\chi+4\pi\eta H_1) = 16\eta H_1/3(\mu+4\pi\eta H_1) \qquad (6)$$

The response of a susceptibility bridge is proportional to the magnetic flux through the specimen and hence to B. A quadrature component $B_\omega \sin\delta$ is introduced due to the phase lag δ. The apparent magnetisation is proportional to the change in the in-phase component $B_\omega \cos\delta - H_1$. From the Fourier analysis it emerges that

$$B_\omega \cos\delta = H_1(1+4\pi\chi+4\pi\eta H_1) \qquad (7)$$

and therefore as H_1 is increased the J-H relationship determined from the AC bridge is identical to (1). This behaviour is quite different from the effects of specimen conductivity, which also introduces a quadrature component, but which also tends to reduce the amplitude of the in-phase component. The response to conductivity is frequency dependent, in contrast to the effects of hysteresis. We have implicitly

assumed the magnetisation to be time-independent - the presence of magnetic viscosity would invalidate these conclusions and lead to a frequency-dependent susceptibility.

From the J-H data a least squares best fit quadratic polynomial was calculated for each specimen. The ratio η/χ was derived directly from the polynomial coefficients. Absolute values of η were then obtained from the measurements of apparent susceptibilities on the calibrated susceptibility bridge. The results are given in Table 2. Initial susceptibility values range from ~0.02 to ~0.01 and η/χ ratios vary between ~3×10^{-2} oe^{-1} and 3×10^{-3} oe^{-1}. Therefore the initial magnetisation curves up to 5 - 10 oe are reasonably linear, and measurements of χ in fields of this order are satisfactory for estimation of susceptibility in the Earth's field ($\sim$0.5 oe).

The absolute calibration of susceptibility is believed accurate to within 1%. An estimate of the probable error in the η/χ ratios and hence in η can be made by considering data on the paramagnetic salt $MnSO_4.H_2O$ for which the magnetisation should be strictly linear in applied fields of this order. The empirical value of η/χ obtained was 3×10^{-4} oe^{-1}, which therefore represents the limit of resolution for η/χ ratios using this instrumentation.

4. SATURATION MAGNETISATION

A Faraday-type balance (Parry, 1967) with a force transducer was used for accurate measurement of magnetisation-applied field relationships. Faceted pole pieces provided an essentially uniform field gradient dH/dz over the specimen producing a force F proportional to J(dH/dz), and therefore to JH. The balance was calibrated using $MnSO_4.H_2O$ in the form of a specimen equal in shape and volume to the synthetic pyrrhotite specimens. In the case of a paramagnetic substance such as manganous sulphate the force is proportional to χmH^2, where χ is the specific susceptibility and m the mass of the substance. This relationship was verified from H = 0 to H = 8.5koe, the maximum field obtainable with this electromagnet and pole configuration.

The magnetisation of ferro- and ferrimagnetic substances obeys the relationship $J = J_s(1-b/H^2)$ to a good approximation in the region of approach to saturation (Chikazumi and Charap, 1978, p.274 ff). The parameter b is related to anistropy constants.

The synthetic pyrrhotite specimens were found experimentally to follow this law of approach to saturation from approximately 6.5koe to 8.5koe. J_s was then obtained by extrapolation of the linear segments of the F/H vs $1/H^2$ plots to $1/H^2 = 0$.

The empirical values for J_s, normalised to unit mass of the sized pyrrhotite fractions, are given in Table 3. together with values of b. The mean of the 9 values of b obtained for distinct grain-size fractions is 6.6×10^6 with standard deviation 0.7×10^6. There is no evidence of a systematic variation of b with grain size, with the possible

exception of the smallest grains. This implies that the anistropy controlling rotation of magnetic moments is essentially the same throughout the grain-size range 6μm - 80μm. For the finest grains the value of b obtained is 10.79×10^6 which is almost three standard deviations from the mean of the values for the other grain sizes. Excluding this outlying value from consideration the mean value of b is then 6.08×10^6, with standard deviation 1.61×10^6. The presence of superparamagnetic grains in R18 would invalidate the assumed form of approach to saturation, as the relationship applicable to superparamagnetic grains involves a $1/H$ term, rather than $1/H^2$ (Bean and Livingston, 1959). This may account for the anomalously high value of b obtained for R18, particularly in view of other hysteresis properties which indicate a superparamagnetic component in R18 (see Section 5).

An alternative, somewhat higher, value of J_s for R18 was obtained by extrapolation of an approximately linear relationship between J and 1/H in moderate fields (up to 8.3koe), and is given in parentheses in Table 3. The true value of J_s for this specimen should presumably lie between the two values. Attempts to fit a quadratic polynomial in 1/H to the J-H data were unsuccessful as the solutions were unstable.

5. HYSTERESIS PROPERTIES

Hysteresis loops (J-H) in fields up to 6.3kG were determined using a Faraday-type balance. In this case the electromagnet was fitted with flat pole pieces to provide a uniform horizontal field over the specimen and a constant, essentially

uniform vertical gradient was produced by specially wound coils on the pole pieces. Bulk coercive force H_c was determined with a precision (and accuracy) of ~2%. Initial susceptibility, saturation magnetisation and saturation remanence were also estimated from the hysteresis loops, but more precise determinations could be made by alternative methods.

Much higher fields, up to 11.6koe, were obtainable with the electromagnet when there was no requirement for a superimposed gradient. All specimens were initially demagnetised (in an alternating field) and then subjected to successively higher steady fields. After each step the isothermal remanence produced was measured with a Digico spinner rock magnetometer. Following saturation of the specimen, successively higher reverse fields were applied and the DC demagnetisation curve determined. After saturation in the reverse direction, the initial process was repeated, producing an essentially symmetrical remanent hysteresis loop (J_r-H). Representative initial remanence acquisition curves and remanent hysteresis loops are shown in Fig. 3 and Fig. 4. The coercivity of remanence H_{cr} defined as the DC back field which is just sufficient to totally demagnetise saturation remanence, increases systematically with decreasing grain size, from 185-190 oe for the NRC (~80μm) specimens to 1245 oe for R18 ($\leq$3μm). It can also be seen from the curves that whereas the remanence for NRC is saturated in ~2 koe, the finest grain sizes do not saturate until considerably higher fields are attained (~5 koe for R18).

Another useful parameter characterising magnetic hardness

is the coercivity of remanence acquisition H'_{cr} , which is defined as the applied field, acting on an initially demagnetised specimen, required to produce a remanance equal to 50% of the saturation value.

Following resaturation and measurement of saturation remanence, J_{rs}, all specimens were subject to alternating field (AF) demagnetisation in successively higher peak fields. AF demagnetisation curves were determined in this way, both for demagnetisation along the axis of magnetisation only (single-axis demagnetisation) and for tumbling AF demagnetisation, where all directions in the specimen are exposed more or less equally to the peak field by making use of a 3-axis quasi-random tumbling system. The median destructive field of saturation remanence is the peak AF which destroys half the remanence. As tumbling AF demagnetisation is more effective than single-axis demagnetisation, the mdf is lower for tumbling than for single-axis demagnetisation.

The (tumbling) AF demagnetisation curves for representative specimens are shown in Fig. 5. AF coercivity spectra derived from these curves (Figs. 6 and 7) indicate a broad range of coercivities in all specimens, but with a very distinct tendency towards higher coercivities with decreasing grain size.

The measured values of the various coercivity parameters H_c, H_{cr}, H'_{cr} and $H_{\frac{1}{2}}$ (for both tumbling and single-axis demagnetisation) are given in Table 4.

The data of Table 4 indicate that pyrrhotite grains smaller than ~100μm are quite magnetically hard. The values of the various coercivity parameters are substantially greater than those for titanomagnetite grains of the same size (e.g. Day et al., 1977). In particular the coercive force of pyrrhotite grains smaller than ~10μm is comparable to that of acicular single domain titanomagnetite grains. These facts have important ramifications for palaeomagnetism of pyrrhotite-bearing rocks and for magnetic interpretation in areas of pyrrhotitic mineralisation, as magnetic hardness is directly related to the capacity to retain stable, ancient and intense remanence.

In common with other magnetic materials coercive force is found to increase markedly with decreasing grain size, d. A bilogarithmic plot of H_c vs d is shown in Fig. 8. In the range 83μm - 11μm the data satisfy the relationship $H_c \propto d^{-n}$, with n= 0.79. According to Stacey and Banerjee (1974, pp.66-69) n is related to domain structure and to the the distribution of crystal defects which impede domain wall motion.

Saturation remanence, J_{rs}, was measured on a Digico fluxgate spinner magnetometer calibrated against the A.N.U. cryogenic (SQUID) magnetometer in Canberra. The cryogenic magnetometer in turn had been calibrated with a current-carrying coil. Calculation of absolute values of J_{rs} for the pyrrhotite required determination of the true mass of pyrrhotite in each specimen. Taking the spontaneous magnetisation of

monoclinic pyrrhotite as 20.3 emu/g (Besnus, 1966), and assuming that the applied fields (<10koe) could not pull the spontaneous magnetisation significantly out of the basal plane, the saturation magnetisation of a randomly oriented assemblage is equal to 20.3 x (π/4) = 15.94 emu/g. Differences between spontaneous and saturation magnetisation intensities are negligible at ambient temperatures in fields of this order, as is shown by the molecular field theory calculations of Besnus et al. (1968).

The true pyrrhotite content of each specimen was then determined from its saturation magnetisation. After normalisation of J_s to 15.94 emu/g the corresponding values of J_{rs} are given in Table 5. The relative remanence ratios, J_{rs}/J_s, are independent of this normalisation, as are the values of χ_m/J_s.

Fields <6koe were sufficient to saturate the remanence of all specimens and the relative remanence ratios are therefore considered to represent saturation values. Viscous decay of saturation remanence was negligible for periods up to several days.

Hysteresis properties are frequently used for characterisation of domain structure and for granulometry of magnetic minerals. Properties which are strongly dependent on grain size are best suited to this sort of analysis. While hysteresis properties are very useful as a tool for qualitative granulometry, semi-quantitative analysis requires more detailed data on the sensitivity of various properties to broad or distinctly bimodal grain size distributions. For example, H_c is more sensitive than H_{cr} to the soft fraction in a mixture of hard

and soft grains (Day et al., 1976; Parry, 1982).

In general, extensive (as opposed to intensive) properties are not particularly useful for magnetic granulometry of rocks because the magnetic mineral concentration is not known *a priori*. Apart from the relatively minor effects of grain interactions, the quantities J_{rs}/J_s, χ/J_s and H_{cr}/H_c are independent of magnetic mineral content. Dunlop (1981) has discussed application of these parameters to analysis of domain structure in titanomagnetites. J_{rs}/J_s decreases from ~0.5 for single domain (SD) titanomagnetite grains to <0.1 for large multidomain (MD) grains, while H_{cr}/H_c increases from <2 to ~5 over the same size range.

Low values of J_{rs}/J_s also pertain to ultrafine grains if a significant superparamagnetic (SPM) fraction is present. Very high values of H_{cr}/H_c (>10) are diagnostic of a SPM fraction. χ/J_s is relatively insensitive to grain size for MD and stable SD magnetite grains ($\chi/J_s \sim 5 \times 10^{-4}$ oe^{-1}), but is a sensitive indicator of SPM material, for which the values are one or two orders of magnitude higher.

It can be seen from Table 5 that for pyrrhotite these three parameters vary systematically with grain size, but that the variation is not spectacular. As will be discussed in another report, the comparatively weak grain size dependence of these parameters reflects the magnetic hardness of pyrrhotite relative to magnetite. Overall the properties of MD grains approach those of SD grains in magnetic materials which are intrinsically hard. The lower spontaneous magnetisation and higher coercive force of pyrrhotite combine to raise J_{rs}/J_s, lower intrinsic susceptibility and reduce H_{cr}/H_c.

Theoretical considerations and the domain structure observations of Soffel (1977, 1981) demonstrate that the critical SD size for pyrrhotite (~2μm) is much larger than for magnetite, as is the domain wall spacing for grains containing several domains. We expect the magnetic properties of pyrrhotite grains to resemble most closely those of smaller, and therefore harder, magnetite grains containing the same number of domain walls. This expectation is supported by the data of Day et al. (1977) which reveal the same trend for small MD titanomagnetite grains. For a fixed grain size, the coercivity (*sensu lato*) increases with titanium content as J_s decreases and the critical size correspondingly augments.

The specimen containing the finest grains, R18, is anomalous in several respects. This specimen should contain only SD and two-domain (TD) grains and should have the highest coercive force, an expectation borne out by the measurements (Table 4). However, systematic trends in η, η/χ, J_{rs}/J_s, χ/J_s and H_{cr}/H_c with decreasing grain size are reversed for the finest grain sizes (Tables 2 and 5). These anomalies can be explained by the presence of some SPM material in the finest fraction. It is likely that some very fine grains are clinging to larger grains. Particles smaller than ~0.02 μm are SPM at room temperature and have a susceptibility up to ~0.2, which is larger by factors of 50 and 20 than the susceptibilities of stable SD and small MD grains respectively. As J_s is characteristic of the material (except for particles only a few atomic diameters across), χ/J_s is augmented by the presence of SPM grains.

J_{rs} is zero for non-interacting SPM grains and, although interactions modify somewhat this ideal behaviour, J_{rs}/J_s is clearly diminished by the presence of a significant fraction of SPM material. H_c is measured in an applied field and is therefore very sensitive to the presence of high susceptibility SPM grains, which acquire in a relatively weak reversed field an induced magnetisation sufficient to cancel the residual remanence. Whilst H_c is lowered by the presence of SPM grains, H_{cr} is unaffected by grains which contribute nothing to the total remanence and is therefore insensitive to SPM grains. The overall effect of SPM grains is thus to increase H_{cr}/H_c. The increase in η/χ can be explained by interactions between high susceptibility SPM particles and other (SPM or stable) grains, on the basis of arguments expounded by Chikazumi and Charap (1978, pp.299-301).

Although the effects of SPM grains are most apparent in R18, the measurements suggest that the next finest grain size fraction, R17, may also contain a small amount of SPM material.

Overall it would seem that the hysteresis properties which are most diagnostic of grain size are the various remanent coercivities. Of these, the median destructive field is the most sensitive to grain size.

A number of derived quantities are given in Table 6 for comparison with various theoretical predictions. According to a phenomonelogical theory of Rayleigh's relations in substances for which low field magnetisation processes are dominated by domain wall displacement (Néel, 1942, 1943), χ^2/η is related to the average number m, of potential energy minima traversed by a domain wall during a saturation hysteresis

cycle by $\chi^2/\eta \simeq 0.9\ J_s/m$. Values of m for the pyrrhotite samples range from ~25 to ~110. The theory predicts that the dimensionless quantity $\eta H_c/\chi$ will be of the order of unity and relatively constant for values of m in this range, and this prediction is supported by the data of Table 3.6. The anomalously high value of $\eta H_c/\chi$ for specimen R18 is not surprising as the theory breaks down for grains with SD structure. Values of this quantity are typically in the range 0.5 - 10 for many magnetic substances and the values for pyrrhotite fall well within this range. Although the values of χ and η for dispersed MD grains are reduced from their intrinsic values χ_i and η_i by the effects of self-demagnetisation (Néel, 1955), being attenuated by factors of $(1+N\chi_i)$ and $(1+N\chi_i)^3$ respectively, this effect is small for these pyrrhotite specimens which have relatively low intrinsic susceptibility. N here is the self-demagnetising factor. It is concluded that the experimental results accord reasonably well with Néel's theory of low field hysteresis.

A simplified theory of domain wall displacement (Stacey and Banerjee, 1974, pp.73-74) predicts that the product $\chi_{11} H_c$ should be proportional to $(n/v)A$ where (n/v) is the number of favourably oriented domain walls of area A per unit volume. For a lamellar domain structure the domain spacing increases as $d^{\frac{1}{2}}$, and therefore the number of walls increases as $d/d^{\frac{1}{2}} = d^{\frac{1}{2}}$. A is proportional to d^2, so $(n/v)A$ goes as $(d^{\frac{1}{2}}/d^3)d^2 = d^{-\frac{1}{2}}$.

For the pyrrhotite grains in these specimens the susceptibility is sufficiently low that self-demagnetising effects are minor, and the observed susceptibility

approximates the intrinsic susceptibility. It will be shown in a subsequent report that domain wall displacement dominates magnetisation processes in low fields for these specimens. Thus $\chi \simeq \chi_{11}/3$ and we expect χH_c to vary approximately as $d^{-0.5}$. The experimental value for the exponent is -0.43, in reasonable agreement with the theory.

It is clear from Table 6 that $H'_{cr} + H_{\frac{1}{2}} = 2H_{cr}$ to a very good approximation for these specimens. A theoretical explanation for this relationshipwill be given in a later report. The theory predicts the following relationship between hysteresis properties: $H_{cr} = H_c/(1-\chi_m H_c/J_{rs})$. This equation is also in good accord with the experimental results, as can be seen from Table 6, although there is evidence of a gradual decrease in the ratio of measured to predicted values of H_{cr} for smaller grains.

6. CONCLUSIONS

The magnetic hysteresis properties of monoclinic pyrrhotite are strongly dependent on grain-size. As the grain-size decreases from $\sim$ 80 μm to $\sim$ 2 μm the low-field emu susceptibility decreases from 0.025 to 0.01 and the coercive force correspondingly increases from 135 oe to 920 oe. Initial magnetisation curves are reasonably linear in fields up to 5-10 oe, implying that susceptibility measurements in fields of this order are satisfactory for petrophysical measurements intended as estimates of susceptibility in the Earth's field.

The magnetic hardness of medium and fine-grained pyrrhotite is correlated with intensity and stability of

remanence. This accounts for the strong remanent magnetisation, often oblique to the present field, commonly carried by pyrrhotite-bearing rocks.

The results given herein establish a framework whereby monoclinic pyrrhotite content and grain-size in rocks can be determined by hysteresis property measurements and provide an empirical basis for theoretical analysis of the rock magnetism of monoclinic pyrrhotite, about which very little is known.

7. ACKNOWLEDGEMENTS

I am grateful to Mr Harry Brown for his assistance in preparation of the sized pyrrhotite fractions.

8. REFERENCES

Bean, C.P. and Livingston, J.D., 1959. Superparamagnetism. J. Appl. Phys., 30: 120S-129S.

Besnus, M.J., 1966. Propriétés magnétiques de la pyrrhotine naturelle. Thesis, University of Strasbourg.

Chikazumi, S. and Charap, S.H., 1978. Physics of Magnetism. Krieger, N.Y., 544 pp.

Day, R., Fuller, M. and Schmidt, V.A., 1976. Magnetic hysteresis properties of synthetic titanomagnetites. J. Geophys. Res., 81: 873-880.

Day, R., Fuller, M. and Schmidt, V.A., 1977. Hysteresis properties of titanomagnetites: grain-size and compositional dependence. Phys. Earth Planet. Inter., 13: 260-267.

Dunlop, D.J., 1981. The rock magnetism of fine particles. Phys. Earth Planet. Inter., 26: 1-26.

Néel, L., 1942. Théorie des lois d'aimantation de Lord Rayleigh, I. Les déplacements d'une paroi isolée. Cahiers de Physique, 12: 1-20.

Néel, L., 1943. Théorie des lois d'aimantation de Lord Rayleigh, II. Multiples domaines et champ coercitif. Cahiers de Physique, 13: 1-13.

Néel, L., 1955. Some theoretical aspects of rock magnetism. Adv. Phys., 4: 191-243.

Parry, J.H., 1967. Principles of magnetic balances. In: D.W. Collinson, K.M. Creer and S.K. Runcorn (Editors). Methods in Palaeomagnetism. Elsevier, pp. 431-437.

Parry, L.G., 1982. Magnetization of immobilized particle dispersions with two distinct particle sizes. Phys. Earth Planet. Inter., 28: 230-241.

Soffel, H., 1977. Pseudo-single-domain effects and single-domain multidomain transition in natural pyrrhotite deduced from domain structure observations. J. Geophys., 42: 351-359.

Soffel, H.C., 1981. Domain structure of natural fine-grained pyrrhotite in a rock matrix (diabase). Phys. Earth Planet. Inter., 26: 98-106.

Stacey, F.D. and Banerjee, S.K., 1974. The Physical Principles of Rock Magnetism. Elsevier, 195 pp.

APPENDIX

PETROGRAPHIC DESCRIPTION OF MT BONNIE ORE

"Massive granular pyrrhotite with a weak foliation and pronounced orientation fabric. Optically only one pyrrhotite is visible...etching is needed to distinguish (petrographically) any hexagonal from monoclinic pyrrhotite.

The slide shows an essentially metamorphic texture with individual pyrrhotite grains frequently slightly elongated along the foliation, and commonly an internal irregular lamellar structure, usually across the smaller dimension. The simple straight to arcuate grain boundaries are invariably fractured in the polished section, while some fractures also bisect individual grains.

The medium to fine grain-size (2 to ¼mm) exceeds that of the minor minerals within the ore, except for some sphalerite. These minor phases are sphalerite, carbonate, 'arsenopyrite', chalcopyrite, galena, 'marcasite' and a rare eutectoid-like reaction intergrowth. While 'arsenopyrite' is euhedral against pyrrhotite, the other minerals occur along grain boundaries and at boundary junctions of the pyrrhotite. This essentially interstitial texture, which indicates a boundary equilibrium metamorphic origin, is in accordance with the spherical habit of the rare sphalerite grains which lie completely within pyrrhotite crystals. Rarely, very fine-grained euhedral platelets of pyrrhotite are present within the carbonate.

The minor phases have an overall elongation subparallel to the foliation. Some, especially 'arsenopyrite', occur in clusters, forming short layers parallel to the foliation. These clusters are quite sporadically concentrated through the pyrrhotite, occurring both as aggregates of more than one mineral and as several disseminated grains. There is a striking local concentration of medium-grained sphalerite in elongated patches extending up to 2mm, cuspate into adjoining pyrrhotite grain boundaries. 'Arsenopyrite' varies in grain-size from 1/3mm to ~10μm. Chalcopyrite rarely occurs as very fine-grained exsolution-type blebs along two planar directions in sphalerite; commonly it occurs separately, or with 'arsenopyrite' (also as exsolution blebs), or as occasional grains with sphalerite. Galena, which is least abundant, is fine-grained and occurs as separate fairly equidimensional grains at pyrrhotite triple junctions, or occasionally as irregular intergrowths with other phases. Pyrite is apparently absent.

TABLE 1 SYNTHETIC DISPERSED PYRRHOTITE SPECIMENS

Specimen	Mean grain size (s.d) (μm)	Pyrrhotite content*	
		mass (mg)	volume %
NRC1	83(38)	39.2	0.08
NRC2	" "	213.0	0.43
NRC3	" "	124.3	0.25
NRF	44(12)	39.7	0.08
R4	42(12)	78.6	0.16
R8	32(8.5)	104.4	0.21
R12	20(6.0)	103.8	0.21
R14	15.5(5.7)	253.4	0.51
R16	11.1(3.4)	98.5	0.20
R17	6.9(1.7)	117.3	0.24
R18	≤3	49.0	0.10

*The quoted mass is that of the magnetic separate prepared from crushed pyrrhotite ore, and therefore includes the mass of contaminants (non-magnetic sulphide and gangue minerals). Assuming the magnetic separate is all pyrrhotite, volume percentages are calculated using a density of 4.6 g/cm^3 and a specimen volume of 10.8 cm^3.

TABLE 2 INITIAL SUSCEPTIBILITIES (χ) AND RAYLEIGH PARAMETERS (η)

Specimen	χ (G/oe)	η (G/oe^2)	η/χ (oe^{-1})
NRC1 (83)	2.61×10^{-2}	8.7×10^{-4}	3.3×10^{-2}
NRC2 (83)	2.41×10^{-2}	5.8×10^{-4}	2.4×10^{-2}
NRC3 (83)	2.37×10^{-2}	5.5×10^{-4}	2.3×10^{-2}
NRF (44)	1.57×10^{-2}	3.3×10^{-4}	2.1×10^{-2}
R4 (42)	1.75×10^{-2}	3.3×10^{-4}	1.9×10^{-2}
R8 (32)	1.50×10^{-2}	2.7×10^{-4}	1.8×10^{-2}
R12 (20)	1.29×10^{-2}	1.8×10^{-4}	1.4×10^{-2}
R14 (15.5)	1.26×10^{-2}	7.8×10^{-5}	6.2×10^{-3}
R16 (11.1)	1.08×10^{-2}	3.5×10^{-5}	3.2×10^{-3}
R17 (6.9)	1.04×10^{-2}	7.1×10^{-5}	6.8×10^{-3}
R18 (<3)	1.19×10^{-2}	1.4×10^{-4}	1.1×10^{-2}

Notes:

1. Quoted values of χ and η are normalised to unit volume of pyrrhotite. The pyrrhotite content of each specimen was determined from the saturation magnetisation.

2. Mean grain sizes in microns are given in parentheses in Tables 2 - 6.

TABLE 3 APPROACH TO SATURATION

Specimen		J'_s (emu/g)	$b.10^{-6}$ (G^2)
NRC1	(83)	13.72	5.92
NRC2	(83)	14.37	5.93
NRC3	(83)	14.54	5.48
NRF	(44)	15.24	7.75
R4	(42)	14.42	4.99
R8	(32)	13.68	7.43
R12	(20)	13.53	7.26
R14	(15.5)	12.15	3.76
R16	(11.1)	11.49	4.19
R17	(6.9)	8.80	7.50
R18	(<3)	7.16(8.34)*	10.79

*Value in parentheses determined from linear extrapolation of J vs 1/H to 1/H = 0.

J'_s = apparent saturation magnetisation.

Law of approach to saturation: $J' = J'_s (1-b/H^2)$

TABLE 4 COERCIVITY PARAMETERS

Specimen	H_c	H_{cr}	H'_{cr}	$H_{\frac{1}{2}}$	$H'_{\frac{1}{2}}$
NRC1 (83)	135	185	270	95	60
NRC2 (83)	140	185	270	100	55
NRC3 (83)	130	190	270	100	55
NRF (44)	210	285	400	185	105
R4 (42)	230	300	400	195	115
R8 (32)	280	340	440	235	130
R12 (20)	375	415	520	340	205
R14 (15.5)	510	520	630	490	270
R16 (11.1)	665	715	790	700	350
R17 (6.9)	825	855	940	740	525
R18 (<3)	920	1245	1340	1120	630

H_c = bulk coercive force

H_{cr} = coercivity of remanence

H'_{cr} = coercivity of remanence acquisition

$H_{\frac{1}{2}}$ = median destructive alternating field (single-axis)

$H'_{\frac{1}{2}}$ = median destructive alternating field (tumbling)

TABLE 5 SATURATION REMANENCE AND HYSTERESIS PROPERTY RATIOS

Specimen	J_{rs} (emu/g)	J_{rs}/J_s	$(\chi_m/J_s)\times10^4$ (oe^{-1})	H_{cr}/H_c
NRC1 (83)	3.81	0.239	3.56	1.37
NRC2 (83)	3.60	0.226	3.29	1.32
NRC3 (83)	3.58	0.225	3.24	1.46
NRF (44)	4.95	0.311	2.15	1.36
R4 (42)	5.51	0.346	2.39	1.30
R8 (32)	6.59	0.413	2.05	1.21
R12 (20)	7.60	0.477	1.76	1.11
R14 (15.5)	9.31	0.584	1.72	1.02
R16 (11.1)	8.43	0.529	1.47	1.08
R17 (6.9)	9.19	0.577	1.42	1.04
R18 (<3)	7.56 (6.49)*	0.474 (0.407)*	1.62 (1.39)*	1.35

J_{rs} = saturation remanence, normalised to unit mass of pyrrhotite

J_s = saturation magnetisation (taken to be 15.94 emu/g)

χ_m = mass susceptibility of pyrrhotite fraction

H_{cr} = coercivity of remanence

H_c = bulk coercive force

*Values in parentheses are calculated using apparent J_s of 8.34 emu/g.

TABLE 6 RELATIONSHIPS BETWEEN HYSTERESIS PROPERTIES

Specimen		χ^2/η (G)	χH_c (G)	$\eta H_c/\chi$	$\frac{H'_{cr}+H_{\frac{1}{2}}}{2H_{cr}}$	$\frac{H_{cr}(J_{rs}-\chi_m H_c}{H_c J_{rs}}$
NRC1	(83)	0.78	3.5	4.5	0.99	1.06
NRC2	(83)	1.00	3.4	3.4	1.00	1.05
NRC3	(83)	1.02	3.1	3.0	0.97	1.19
NRF	(44)	0.75	3.3	4.4	1.02	1.16
R4	(42)	0.93	4.0	4.4	1.00	1.10
R8	(32)	0.83	4.2	5.0	1.00	1.05
R12	(20)	0.92	4.8	5.3	1.04	0.95
R14	(15.5)	2.04	6.4	3.2	1.08	0.87
R16	(11.1)	3.33	7.2	2.2	1.04	0.88
R17	(6.9)	1.52	8.6	5.6	0.98	0.83
R18	(<3)	1.01	11.0	10.1	0.99	0.93
					mean 1.01	mean 1.01
					s.d. 0.03	s.d. 0.12

Fig. 1(a) High-field thermomagnetic (J_s - T) curve for Mt. Bonnie pyrrhotite ore. The heating took place in air. The curve is Weiss-type with Curie temperature 320°C, indicating 4C monoclinic pyrrhotite ($\sim Fe_7S_8$).

1(b) Low-field thermomagnetic (k-T) curve for Mt. Bonnie pyrrhotite ore. The powdered sample was heated in air, but no difference was found for curves obtained by heating in nitrogen or vacuum.

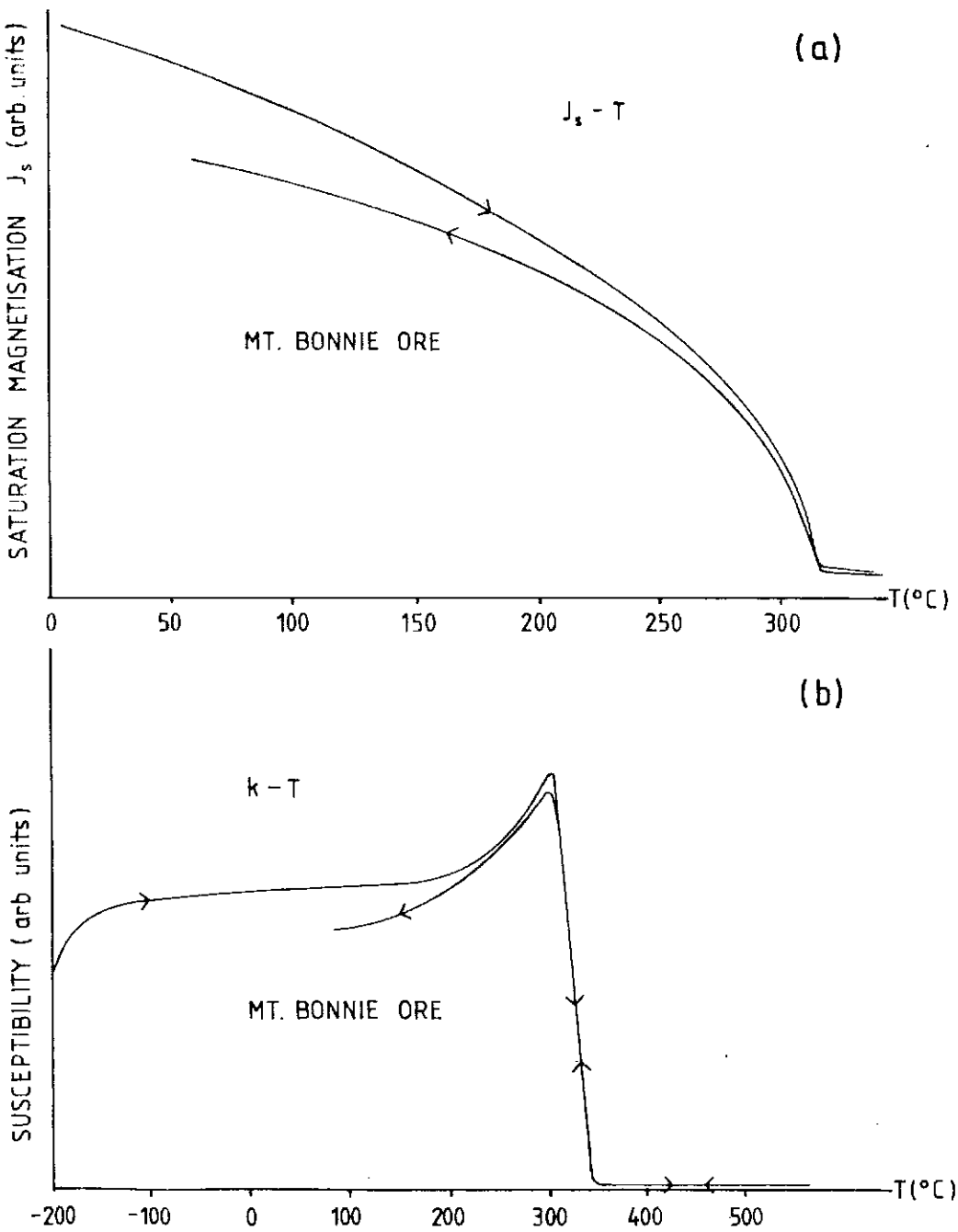
(a)
J_s - T
MT. BONNIE ORE
SATURATION MAGNETISATION J_s (arb. units)
0
50
100
150
200
250
300
T(°C)
(b)
k - T
MT. BONNIE ORE
SUSCEPTIBILITY (arb units)
-200
-100
0
100
200
300
400
500
T(°C)

FIG. 1

Fig. 2 Photomicrographs of grains from sized pyrrhotite fractions. Top: R4 (mean grain size 42μm). The field of view is 480μm x 340μm. Bottom: R17 (mean grain size 6.9μm). The field of view is 300μm x 210μm.

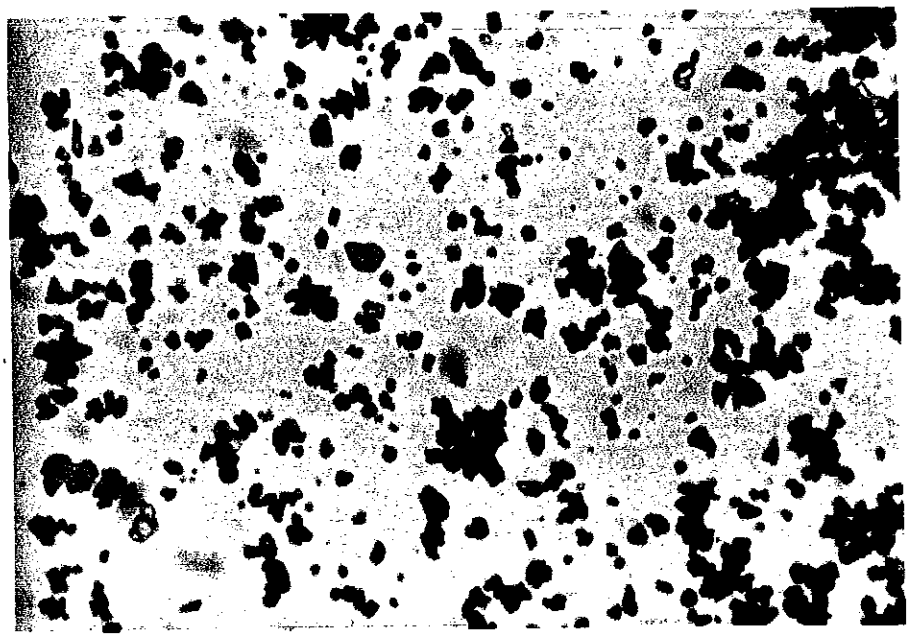

FIG. 2

Fig. 3 Initial remanence acquisition curves and remanent hysteresis loops for specimens NRC, R4, R8 and R12. An initially demagnetised specimen (at the origin of the plot) was subjected to successively higher applied fields, H, until it was saturated in the forward direction. After each exposure to a field the specimen was removed from the electromagnet and its remanence, J_r, measured to obtain the initial remanence acquisition curve. Following saturation the specimen was subjected to successively higher back-fields producing the left-hand branch of the remanent hysteresis loop. The symmetrical right-hand branch was produced by again applying forward fields to the specimen saturated in the reversed direction.

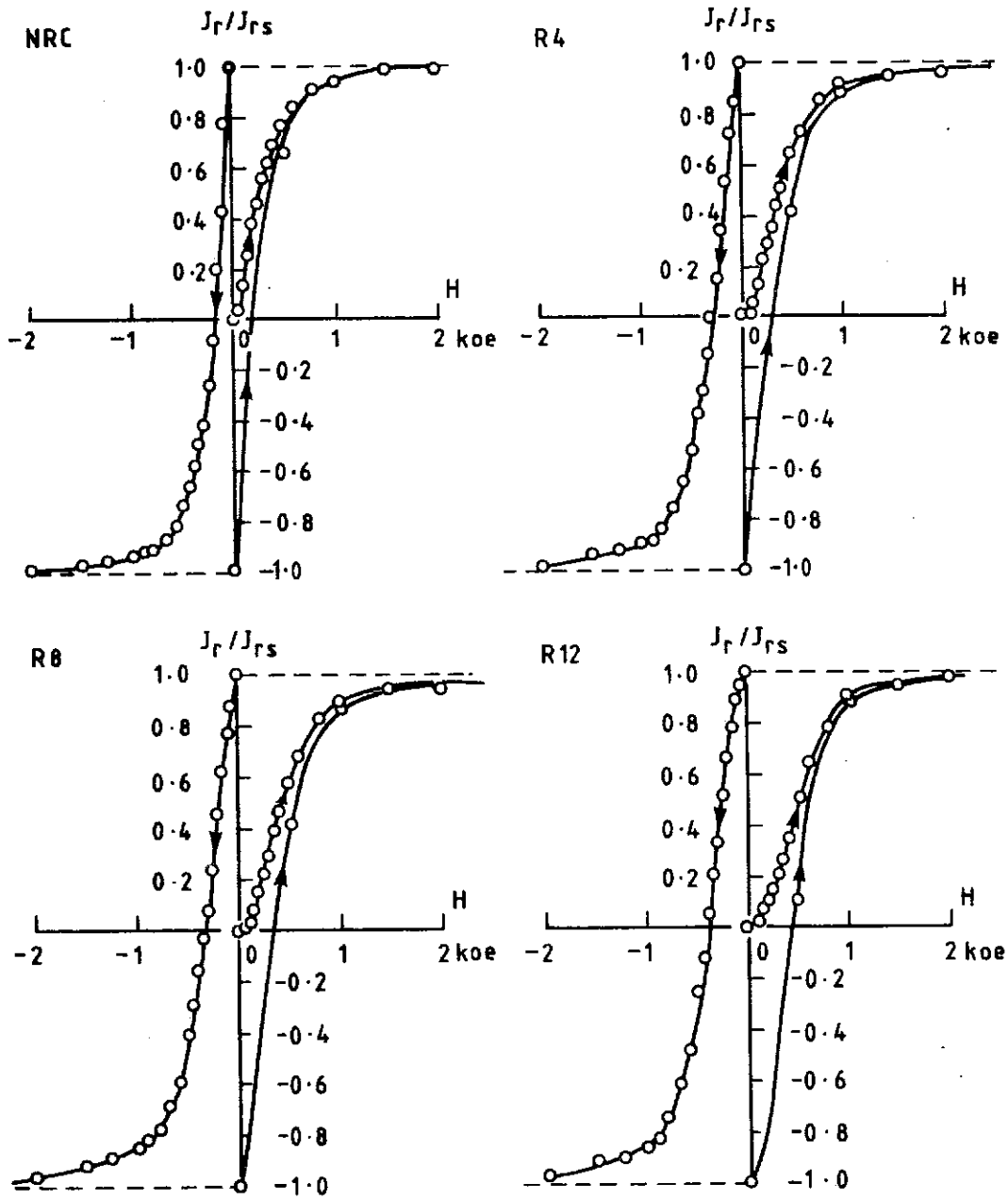
NRC
J_r/J_{rs}
1·0
0·8
0·6
0·4
0·2
H
−2
−1
0
1
2 koe
−0·2
−0·4
−0·6
−0·8
−1·0
R4
J_r/J_{rs}
R8
J_r/J_{rs}
R12
J_r/J_{rs}

FIG. 3

Fig. 4 Initial remanence acquisition curves and remanent hysteresis loops for specimens R14, R16, R17 and R18.

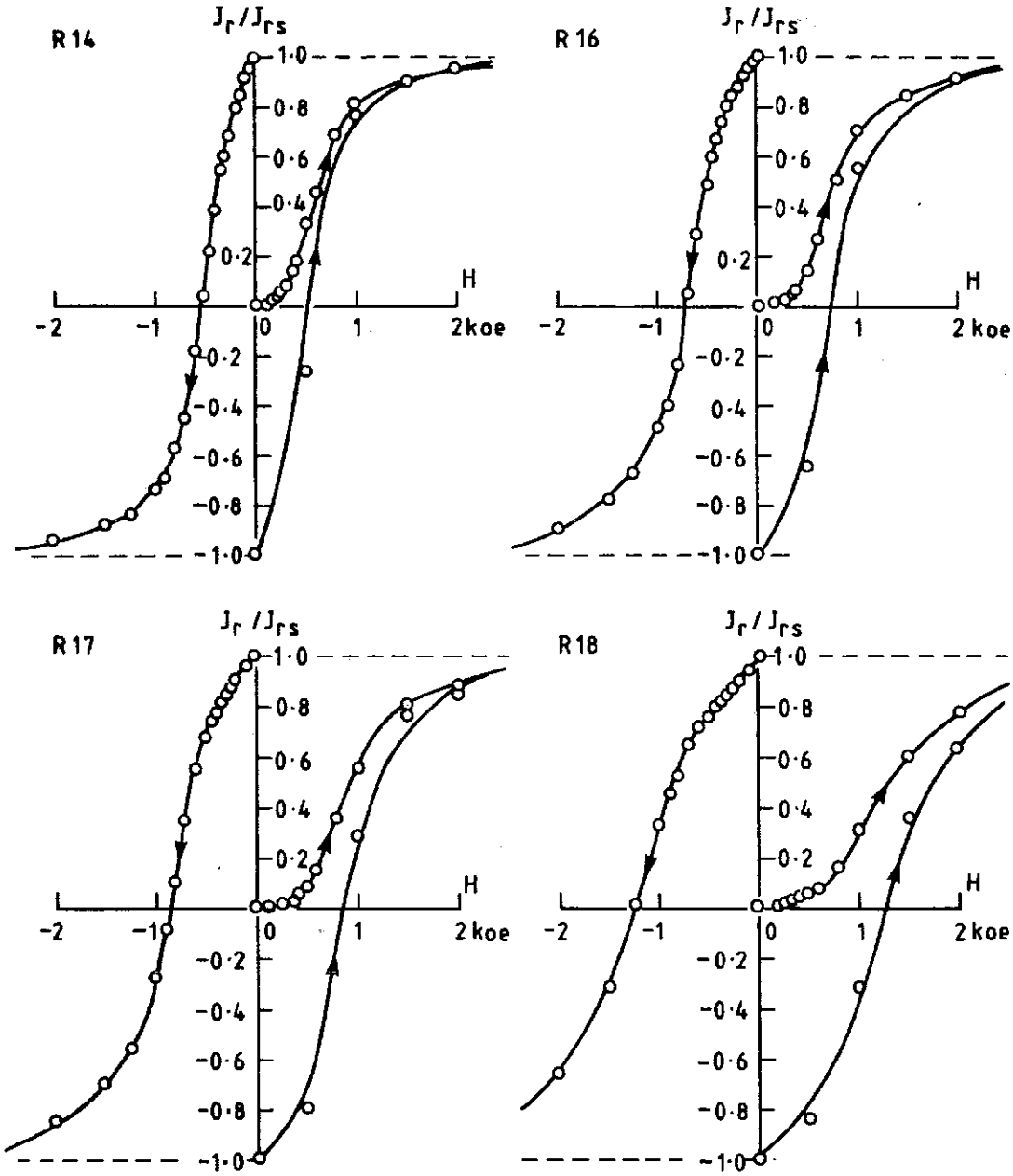
R 14
J_r / J_{rs}
1·0
0·8
0·6
0·4
0·2
-0·2
-0·4
-0·6
-0·8
-1·0
H
-2
-1
0
1
2koe
R 16
J_r / J_{rs}
1·0
0·8
0·6
0·4
0·2
-0·2
0·4
-0·6
-0·8
-1·0
H
-2
-1
0
1
2 koe
R 17
J_r / J_{rs}
1·0
0·8
0·6
0·4
0·2
-0·2
-0·4
-0·6
-0·8
-1·0
H
-2
-1
0
1
2 koe
R 18
J_r / J_{rs}
1·0
0·8
0·6
0·4
0·2
-0·2
-0·4
-0·6
-0·8
-1·0
H
-2
-1
0
1
2 koe

FIG. 4

Fig. 5. AF demagnetisation curves of saturation remanence for selected sized pyrrhotite specimens. Demagnetisation was carried out using a 3-axis tumbling system.

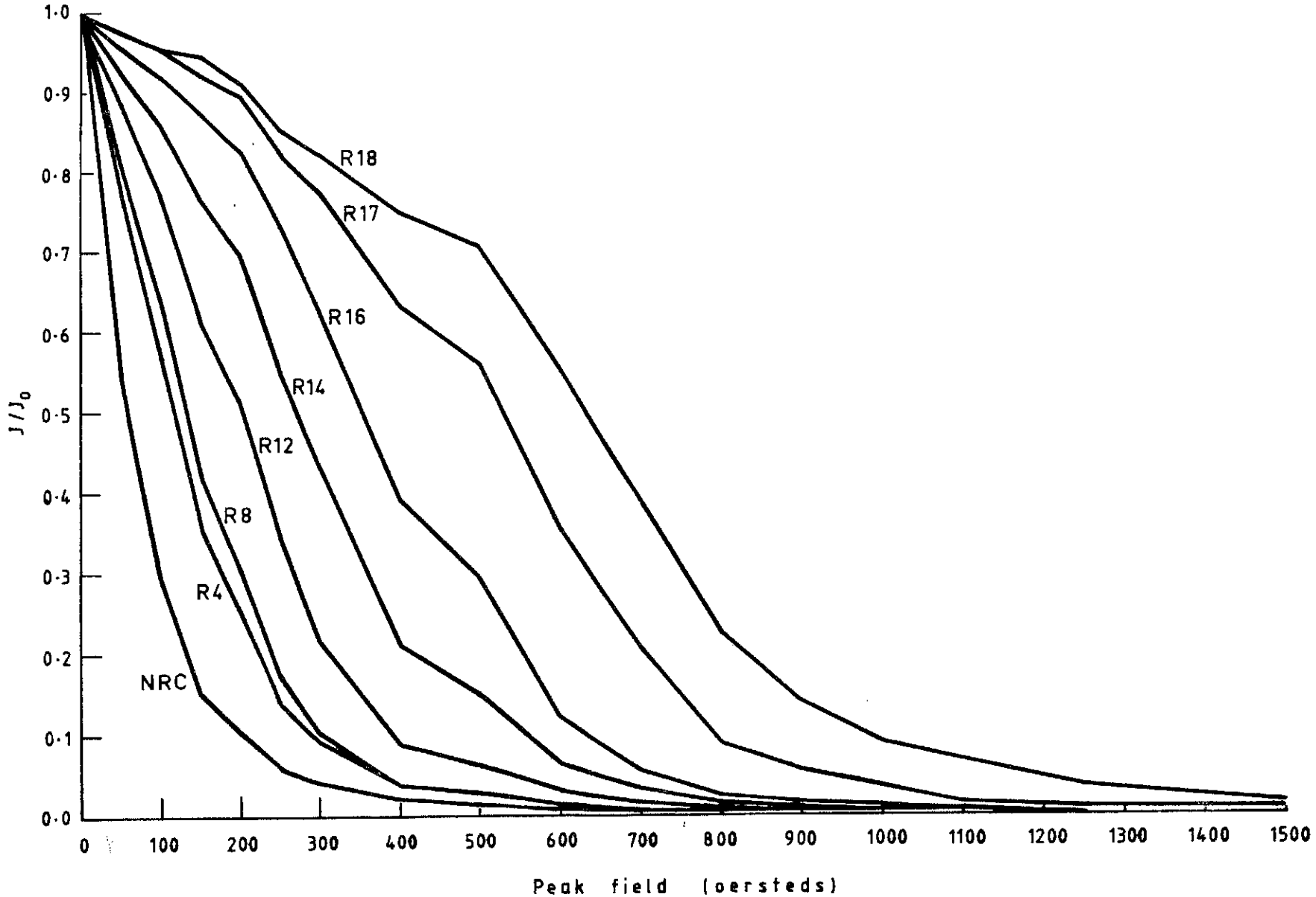

FIG. 5 TUMBLER AF DEMAGNETISATION OF SATURATION IRM

Fig. 6. AF coercivity spectra for specimens NRC, R4, R8 and R12, derived from the AF demagnetisation curves of Fig. 5.

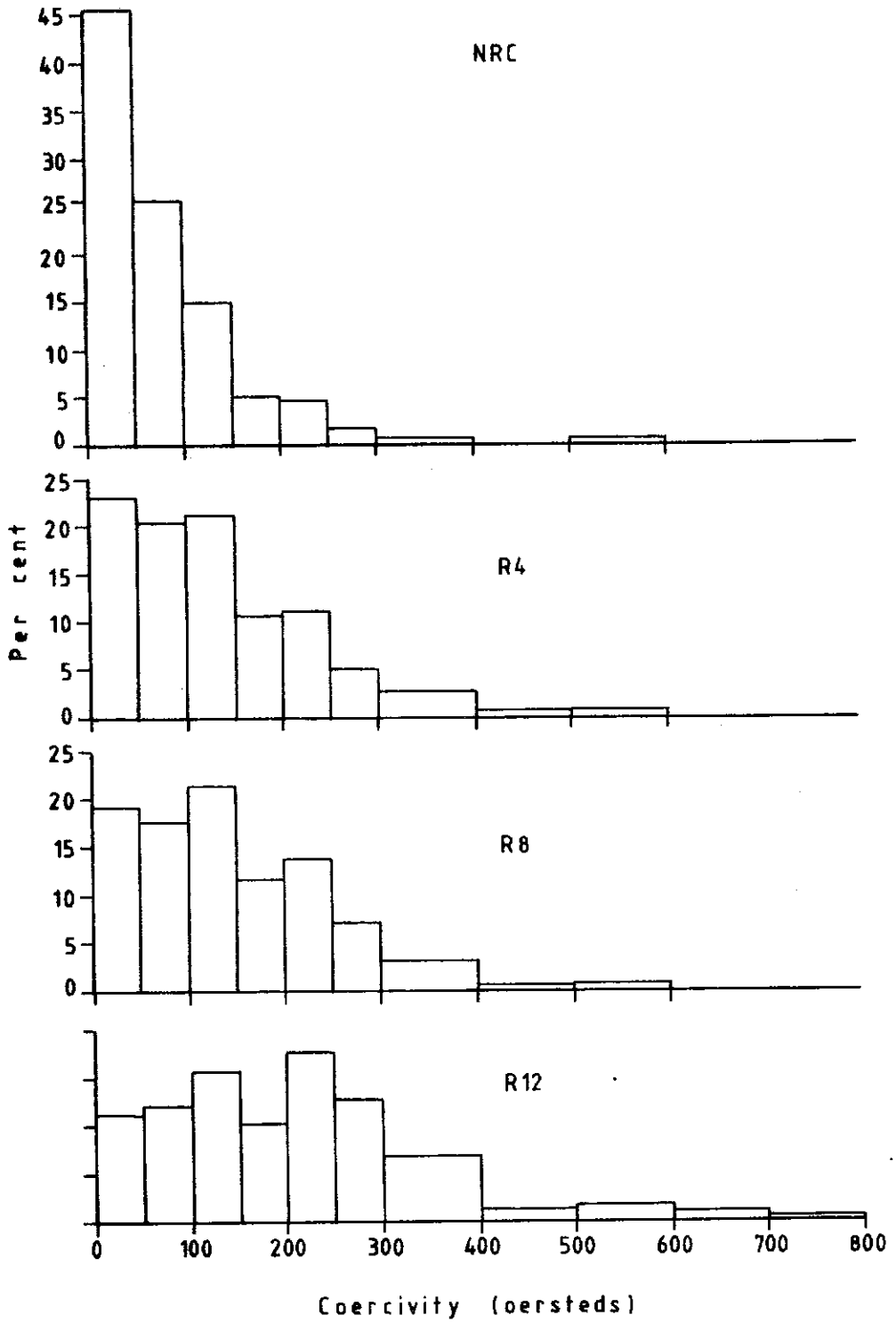

FIG. 6 AF COERCIVITY SPECTRA

Fig. 7. AF coercivity spectra for specimens R14, R16, R17 and R18, derived from the AF demagnetisation curves of Fig. 5.

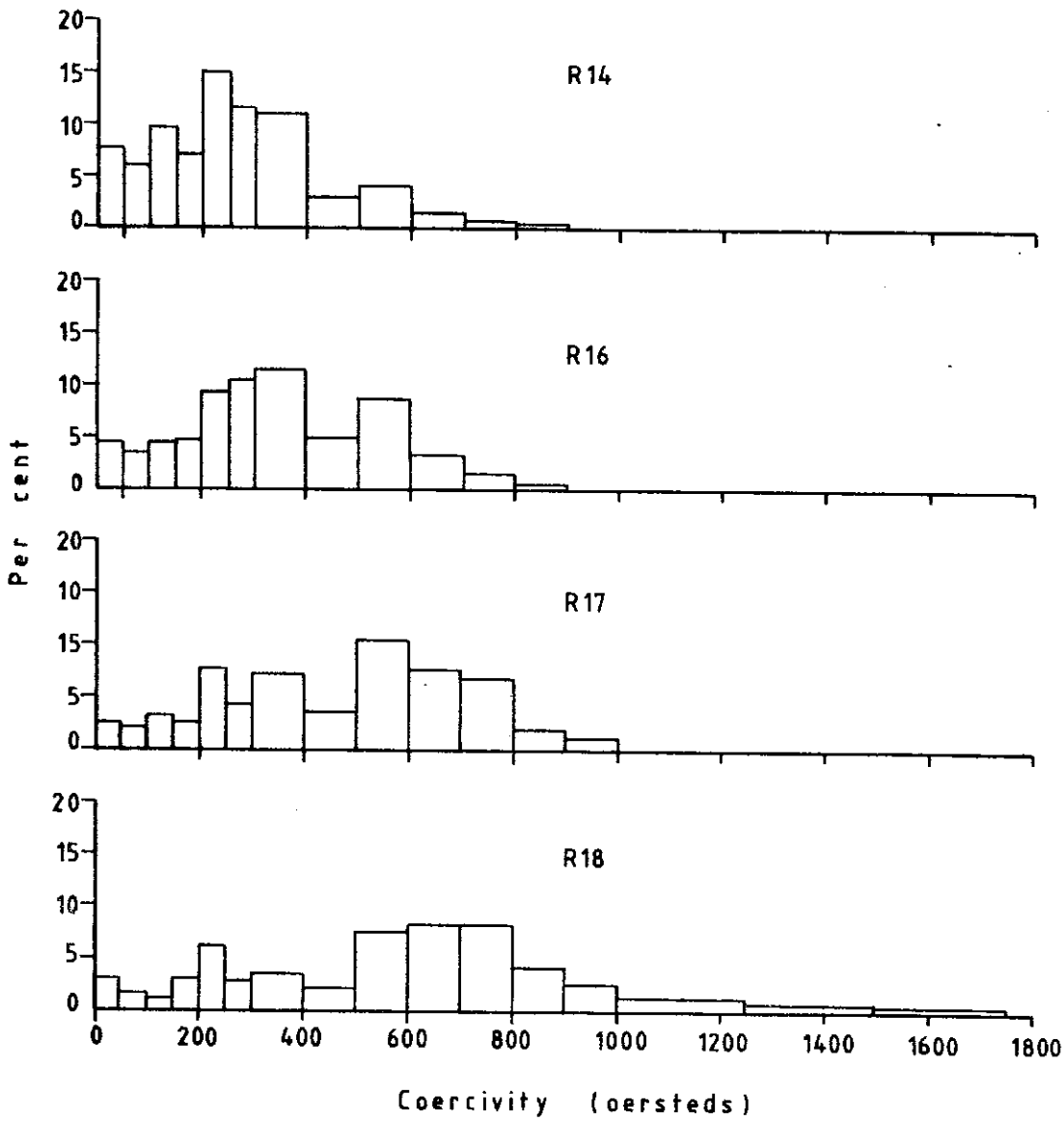

FIG. 7 AF COERCIVITY SPECTRA

Fig. 8 Bilogarithmic plot of coercive force versus grain size for sized pyrrhotite specimens. The straight line corresponds to the relationship $H_c = 4310d^{-0.79}$

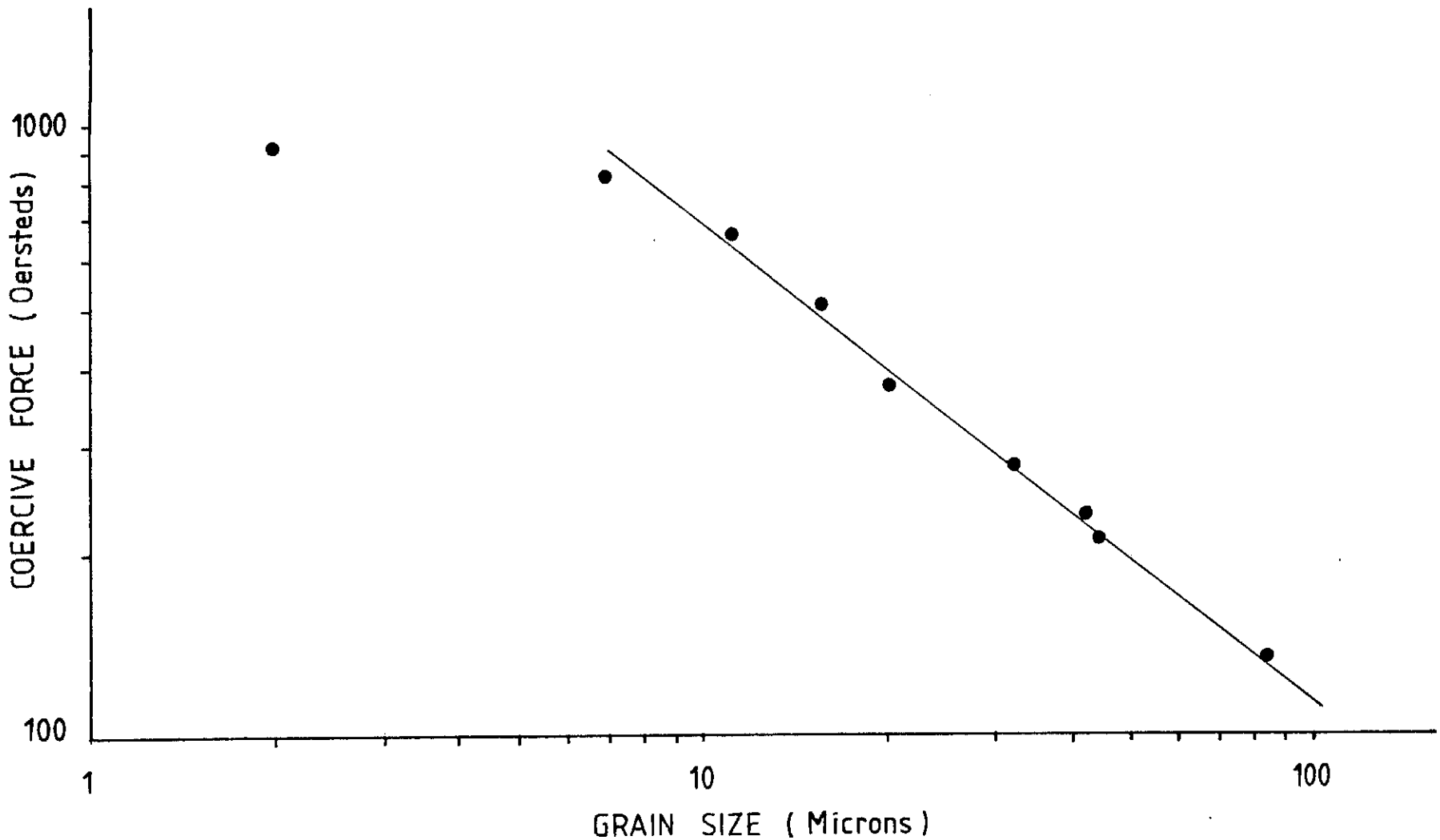
1000
100
COERCIVE FORCE (Oersteds)
1
10
100
GRAIN SIZE (Microns)

FIG. 8